# Synthesis and Characterization of Carbon-Coated $LiNi_{1/3}Co_{1/3}Mn_{1/3}O_2$ in a Single Step by an Inverse Microemulsion Route

**Nupur Nikkan Sinha and N. Munichandraiah***

Department of Inorganic and Physical Chemistry, Indian Institute of Science, Bangalore 560 012, India

**ABSTRACT** Layered $LiNi_{1/3}Co_{1/3}Mn_{1/3}O_2$, which is isostructural to $LiCoO_2$, is considered as a potential cathode material. A layer of carbon coated on the particles improves the electrode performance, which is attributed to an increase of the grain connectivity and also to protection of metal oxide from chemical reaction. The present work involves in situ synthesis of carbon-coated submicrometer-sized particles of $LiNi_{1/3}Co_{1/3}Mn_{1/3}O_2$ in an inverse microemulsion medium in the presence of glucose. The precursor obtained from the reaction is heated in air at 900 °C for 6 h to get crystalline $LiNi_{1/3}Co_{1/3}Mn_{1/3}O_2$. The carbon coating is found to impart porosity as well as higher surface area in relation to bare samples of the compound. The electrochemical characterization studies provide that carbon-coated $LiNi_{1/3}Co_{1/3}Mn_{1/3}O_2$ samples exhibit improved rate capability and cycling performance. The carbon coatings are shown to suppress the capacity fade, which is normally observed for the bare compound. Impedance spectroscopy data provide additional evidence for the beneficial effect of a carbon coating on $LiNi_{1/3}Co_{1/3}Mn_{1/3}O_2$ particles.

**KEYWORDS:** lithium ion cells • cathode material • carbon coating • rate capability

## INTRODUCTION

Lithium ion batteries have become the preferred power sources for portable electronic devices because of their high volumetric and gravimetric energy densities (1). Studies on reversible electrochemical deintercalation/intercalation of $Li^+$ ions from/into $LiCoO_2$ by Goodenough's group (2) were responsible for the development of commercial lithium ion batteries. Studies on $LiCoO_2$ as a positive-electrode material were followed by investigations on several compounds on the basis of compositions such as $LiNiO_2$, $LiMnO_2$, $LiMn_2O_4$, $LiFePO_4$, etc. Recently, the layered $LiNi_{1/3}Co_{1/3}Mn_{1/3}O_2$ oxide was investigated because of its favorable features such as high capacity, structural stability, thermal stability, low cost, safety, etc. (3, 4). Several procedures for the synthesis of $LiNi_{1/3}Co_{1/3}Mn_{1/3}O_2$ are reported in the literature (5−12). Ge et al. (5) prepared $LiNi_{1/3}Mn_{1/3}Co_{1/3}O_2$ by a water-in-oil emulsion method. The required amounts of acetates of Li, Ni, Co, and Mn were dissolved in distilled water and mixed with a large volume of kerosene. After the contents was stirred to get a homogeneous emulsion, it was dropped in hot kerosene (150 °C). The obtained dried material was heated at 400 °C for 1 h followed by calcination at various temperatures ranging from 450 to 850 °C to prepare $LiNi_{1/3}Co_{1/3}Mn_{1/3}O_2$. Other procedures include glycine−nitrate combustion (6), spray drying (7, 8), a wet chemical route (9), coprecipitation followed by heating (10, 11), and a high-temperature solid-state method using metal carbonates (12). In a majority of the studies involving a $LiNi_{1/3}Co_{1/3}Mn_{1/3}O_2$ positive-electrode material, large particles are synthesized and studied. The particle size is an important parameter that influences the rate capability of the positive active materials. While small particles can increase the rate capability, nanosized particles can be harmful for battery application because of the high reactivity of nanoparticles with the electrolyte. Therefore, submicrometer-sized particles are desirable because they can be more chemically stable than the nanoparticles and possess greater rate capability than microparticles.

$LiNi_{1/3}Co_{1/3}Mn_{1/3}O_2$ integrates the features of $LiCoO_2$, $LiNiO_2$, and $LiMnO_2$. However, its electronic conductivity is relatively lower than that of $LiCoO_2$ (13). The addition of dopants (14−16) and modification of the surfaces (11, 17−19) of electrode materials were studied to improve the electronic conductivity. In particular, a thin carbon coating on particles is known to be effective not only in enhancing the conductivity of the metal oxide but also in protecting the particles from chemical attack by the electrolyte. As a consequence, diverse methods of carbon coatings such as chemical vapor deposition, pyrolysis of adsorbed organic compounds, etc., were employed (12, 20). All of these methods consist of two steps, the first involving the synthesis of the compound and the second providing carbon coating on the particles at an elevated temperature.

In the present study, $LiNi_{1/3}Co_{1/3}Mn_{1/3}O_2$ is prepared using an inverse microemulsion synthetic route. Submicrometer-sized particles are obtained. Furthermore, a layer of carbon is coated on particles in situ during the synthesis. Carbon-coated $LiNi_{1/3}Co_{1/3}Mn_{1/3}O_2$ submicrometer-sized particles, synthesized in a single step, are found to possess a high rate capability.

* Corresponding author. E-mail: muni@ipc.iisc.ernet.in.
Tel: +91-80-22933183. Fax: +91-80-2360-0683.
Received for review February 25, 2009 and accepted May 5, 2009
DOI: 10.1021/am900120s

## EXPERIMENTAL SECTION

Analytical-grade chemicals, namely, lithium nitrate (Aldrich), nickel nitrate (SD Fine Chemicals), cobalt nitrate (SD Fine Chemicals), manganese nitrate (Aldrich), cyclohexane (Merck), high-purity lithium dodecylsulfate (LDS; Aldrich), *n*-butanol (SD Fine Chemicals), glucose (SD Fine Chemicals), lithium foil of 0.7 mm thickness (Aldrich), poly(vinylidene fluoride) (PVDF; Aldrich), acetylene black (AB; Alfa Aesar), 1-methyl-2-pyrrolidinone (NMP; Aldrich), ethylene carbonate (EC; Aldrich), dimethyl carbonate (DMC; Aldrich), and $LiAsF_6$ (Aldrich) were used as received. Aqueous solutions of metal nitrates were prepared using doubly distilled water. $LiNi_{1/3}Co_{1/3}Mn_{1/3}O_2$ was synthesized from a quaternary microemulsion consisting of water, cyclohexane, LDS, and *n*-butanol. A solution was prepared by mixing 51.2 mL of cyclohexane (oil), 6.2 mL of *n*-butanol (cosurfactant), and 0.225 g of LDS (surfactant) and stirred well until it became optically transparent. To this nonaqueous medium, 15 mL of an aqueous solution consisting of 5 mL each of 0.5 M $M(NO_3)_2$ (where M = Ni, Co, Mn) and 5 mL of 1.8 M $LiNO_3$ was added. This amounts to 20% more lithium than the stoichiometric requirement for the formation of $LiNi_{1/3}Co_{1/3}Mn_{1/3}O_2$. To this emulsion medium were added different amounts of glucose (0.0−1.0 g) as a source for carbon. The emulsion was stirred for 12 h followed by evaporation at 120 °C to obtain a brown gel. The gel was heated at 400 °C in air for 6 h, and a precursor was obtained. The quantity of precursor obtained in a typical batch of synthesis was about 0.9 g. Subsequently, the precursor samples were heated at 900 °C in air for 6 h to get the final products. Samples prepared with 0.0, 0.1, 0.3, 0.5, 0.75, and 1.0 g of glucose are hereafter referred as C0, C0.1, C0.3, C0.5, C0.75, and C1.0, respectively.

For electrochemical characterization, electrodes were prepared on aluminum foil (0.2 mm thick) as a current collector. A circular aluminum foil of area 1 $cm^2$ was polished with successive grades of emery, cleaned with detergent, etched in dilute $HNO_3$, washed with doubly distilled water, rinsed with acetone, dried, and weighed. $LiNi_{1/3}Co_{1/3}Mn_{1/3}O_2$ (80 wt %), AB (15 wt %), and PVDF (5 wt %) were ground in a mortar; a few drops of NMP were added to form a syrup. It was coated onto the pretreated aluminum foil (area 1 $cm^2$) and dried at 110 °C for a few minutes. Coating and drying steps were repeated to get the required loading level (4−6 mg) of the active material. The electrodes were dried at 110 °C under vacuum for 12 h. Finally, the electrodes were pressed at a pressure of 25 kN by a hydraulic press. Electrochemical cells were assembled in homemade Swagelok-type poly(tetrafluoroethylene) cell holders, using a lithium foil for both the counter and reference electrodes. A glass mat soaked in the electrolyte was used as the separator. The electrolyte was 1 M $LiAsF_6$ in 1:1 mixed solvents of EC and DMC. The solvents were repeatedly treated with molecular sieves (4 Å) before preparing the electrolyte. Cells were assembled in an argon-atmosphere glovebox (MBraun model UNILAB).

Powder X-ray diffraction (XRD) patterns were recorded using a Bruker AXS D8 diffractometer with Cu Kα ($\lambda$ = 1.5418 Å) as the source. Thermogravimetric analysis (TGA) data were recorded in the temperature range from ambient to 900 °C at a heating rate of 10 °C $min^{-1}$ in air using Perkin-Elmer thermal analyzer model Pyris Diamond TG/DTA. Microstructures were examined by FEI Co. scanning electron microscope model SIRION and FEI Co. high resolution transmission electron microscope model TECNAI F30. Brunauer−Emmett−Teller (BET) surface area measurements of the samples were carried out using a Micromeritics surface area analyzer model ASAP 2020. X-ray photoelectron spectroscopy (XPS) was carried out on a SPECS photoelectron spectrometer (Phoibos 100 MCD energy analyzer) using monochromatic Mg Kα radiation (1253.6 eV). XPS signals were analyzed using CASA XPS software.

Cyclic voltammograms were recorded with a Biologic SA multichannel potentiostat/galvanostat model VMP3. The impedance spectra were recorded potentiostatically at open-circuit potential with an alternating-current (ac) excitation signal of 5 mV (peak to peak) over a frequency range from 100 kHz to 0.01 Hz using Solartron potentiostat/galvanostat model 1287 in combination with Solartron frequency response analyzer model 1255B. Impedance data were subjected to the nonlinear least-squares (NLLS) fitting procedure. The charge−discharge cycling of the cells was carried out using a Bitrode battery cycle-life tester. Reproducibility of the electrochemical data was ensured by repeating the experiments with at least another electrode of the same sample. Only representative results are presented. All electrochemistry experiments were conducted in an air-conditioned room at 20 ± 2 °C.

## RESULTS AND DISCUSSION

In the inverse microemulsion synthesis, 20 mL of an aqueous solution consisting of $M(NO_3)_2$ (M = Ni, Co, Mn) and $LiNO_3$ with molar ratio Li/M = 1.2 and varying amounts of glucose (0−1.0 g) was dispersed in 51.2 mL of cyclohexane. The aqueous droplets were stabilized by LDS molecules, with their polar head groups oriented toward the aqueous drops and the aliphatic tails toward the organic phase. Intermixing of the reactants took place within the droplets. Slow evaporation of the emulsion resulted in the formation of a gel consisting of metal nitrates in narrow regions, which were surrounded by surfactant molecules. During the subsequent heat treatment, the mixed-metal nitrates as well as the surfactant were oxidized, resulting in the formation of submicrometer-sized particles of $LiNi_{1/3}Co_{1/3}Mn_{1/3}O_2$. The presence of glucose in the reaction medium facilitates the formation of the carbon coating on the surface of the oxide particles. The procedure of Ge et al. (5) involving kerosene appears to be cumbersome, and simpler procedures of the synthesis in a microemulsion medium at lower temperature are preferable. In the present method, cyclohexane was used as the nonaqueous phase and the precursor was obtained by simple evaporation of the emulsion. Furthermore, the addition of glucose in the microemulsion facilitated the formation of carbon layers on particles of the product in a single step, unlike the separate steps adopted in the literature (9, 10). Lin et al. (8) prepared $LiNi_{1/3}Co_{1/3}Mn_{1/3}O_2$ by slurry spray drying using $Li_2CO_3$, NiO, $Co_3O_4$, and $MnCO_3$. Then the particles were dispersed in ethanol consisting of citric acid as the carbon source. The mixture was stirred, dried, and heated at 600 °C to obtain the carbon-coated particles of $LiNi_{1/3}Co_{1/3}Mn_{1/3}O_2$. In another study, Kim et al. (10) prepared the compound by coprecipitation from a solution containing metal sulfates by the addition of an alkaline solution, and then the particles were coated with carbon using gelatin dissolved in water as the carbon source.

Thermal analysis data of a precursor sample is shown in Figure 1. From the TGA trace, there is about 17% weight loss when the sample is heated to 100 °C, which is due to the removal of adsorbed water. Between 290 and 450 °C, about 25% weight loss is due to decomposition of nitrates, surfactants, and glucose. There is no noticeable weight loss between 500 and 900 °C. Thus, the formation of the compound including the carbon coating is expected to take

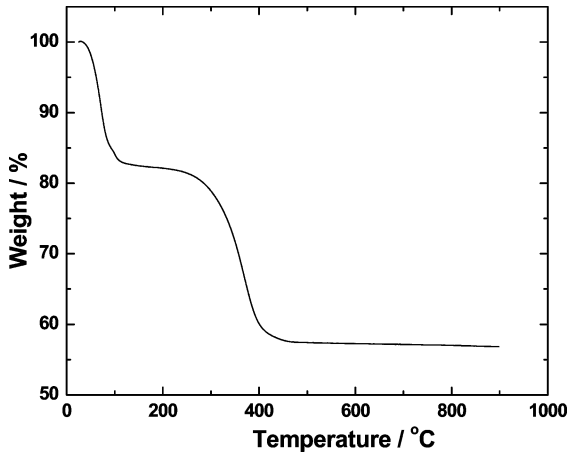


**FIGURE 1. TGA curve of the precursor recorded at a heating rate of 10 °C min$^{-1}$.**

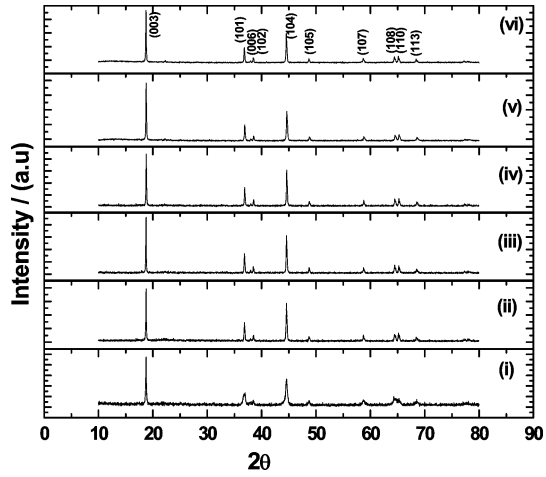


**FIGURE 2. Powder XRD patterns of C0 (i) and carbon-coated (ii) C0.1, (iii) C0.3, (iv) C0.5, (V) C0.75, and (vi) C1.0 samples of $LiNi_{1/3}Co_{1/3}Mn_{1/3}O_2$ obtained by heating of the precursors at 900 °C for 6 h.**

place around 400 °C. Nevertheless, the precursor was heated at 900 °C for 6 h to obtain the crystalline product. Similar TGA curves for precursors made with varying amounts of glucose were recorded.

XRD patterns of the samples prepared with varying amounts of glucose are shown in Figure 2. It is known that $LiNi_{1/3}Co_{1/3}Mn_{1/3}O_2$ has a hexagonal crystal structure of $\alpha$-$NaFeO_2$ with a space group of $R\bar{3}m$ (23). The XRD patterns of all samples agree with the pattern of a pure single phase of $LiNi_{1/3}Co_{1/3}Mn_{1/3}O_2$. The main diffraction peaks, namely, (003), (101), and (104), remain at the same $2\theta$ values for all of the samples. No impurity phase is observed for the samples prepared in the presence of glucose, suggesting that the structure of $LiNi_{1/3}Co_{1/3}Mn_{1/3}O_2$ is unaffected. Because the amount of carbon present on the particle is small, no diffraction peaks corresponding to the crystalline form of carbon are detected. The presence of two pairs of doublet peaks (006)/(102) and (108)/(110) at $2\theta$ = 38° and 65°, respectively, confirms the formation of a well-developed layered structure. Furthermore, the intensity ratio of the (003) and (104) peaks is 1.6. This ratio is sensitive to cation mixing in the lattice. The higher the ratio, the lower the degree of cation mixing (24). Generally, this ratio should be larger than 1.2 for a layered compound with a good electrochemical performance (25). The lattice parameters, $a$ = 2.8587 Å and $c$ = 14.2287 Å, are calculated for the C0 sample. The unit cell parameters calculated from the XRD spectra of the carbon-coated samples are nearly the same as those of the C0 sample. The average values of $a$ = 2.8590 ± 0.004 Å and $c$ = 14.2255 ± 0.0108 Å are calculated for the C0, C0.1, C0.3, C0.75, and C1.0 samples of $LiNi_{1/3}Co_{1/3}Mn_{1/3}O_2$. These values match well with $a$ = 2.687 Å and $c$ = 14.246 Å; (3) $a$ = 2.864 ± 0.005 Å and $c$ = 14.233 ± 0.008 Å; $a$ = 2.872 Å and $c$ = 14.243 Å; (5) $a$ = 2.861 Å and $c$ = 14.240 Å; (6) and $a$ = 2.852 Å and $c$ = 14.208 Å (7) reported in the literature. Thus, the present preparation method employing a microemulsion-derived gel produced layered metal oxides without cation mixing. The presence of glucose in the reaction medium does not alter the crystal structure.

The scanning electron microscopy (SEM) micrographs of the $LiNi_{1/3}Co_{1/3}Mn_{1/3}O_2$ samples prepared with varying amounts of glucose are shown in Figure 3. In all samples, the particle size is in the range from 100 to 200 nm. There is no uniformity in the shape of the particles, although the particles are generally in a polyhedral shape. The synthetic method employed in the present study, namely, the inverse microemulsion route, thus, is useful for the preparation of submicrometer-sized particles of $LiNi_{1/3}Co_{1/3}Mn_{1/3}O_2$ both without and with carbon coatings. The presence of glucose as the source for carbon coating does not exhibit any noticeable influence on the shape, size, and geometry of the particles. The particle size ranging from 0.5 to 2 $\mu$m was reported for the $LiNi_{1/3}Co_{1/3}Mn_{1/3}O_2$ sample prepared by acetate decomposition and spray-drying methods (7). Spongy morphology and irregular agglomerated large particles were obtained by the wet chemical process (8). Irregular-shaped particles of size >1 $\mu$m, carbon-coated samples were synthesized by the spray-drying method (9). For carbon-coated samples by the coprecipitation method (10, 11), agglomerated spherical particles of 10 $\mu$m were observed. In relation to these studies involving large particles, the present inverse microemulsion route yields carbon-coated samples of less than 200 nm particle size. It is interesting to note that another inverse microemulsion route with kerosene as the oil phase (5) also yielded uncoated $LiNi_{1/3}Co_{1/3}Mn_{1/3}O_2$ of an average particle size of about 200 nm. Thus, the inverse microemulsion route is evidently an appropriate route for the preparation of submicrometer-sized particles of $LiNi_{1/3}Co_{1/3}Mn_{1/3}O_2$. The transmission electron microscopy (TEM) images of the C0, C0.1, C0.3, and C0.75 samples of $LiNi_{1/3}Co_{1/3}Mn_{1/3}O_2$ particles are shown in Figure 4. It is clearly seen that a layer of carbon is coated on the surface of the $LiNi_{1/3}Co_{1/3}Mn_{1/3}O_2$ particle (Figure 4B–D) and the thickness of the coating has slightly increased from part B to part D of Figure 4. Such a type of coating is not present on the particle of the C0 sample. Similar TEM micrographs showing the layers of carbon coatings were reported (26). It is found that formation of the free carbon powder also occurs in addition to the

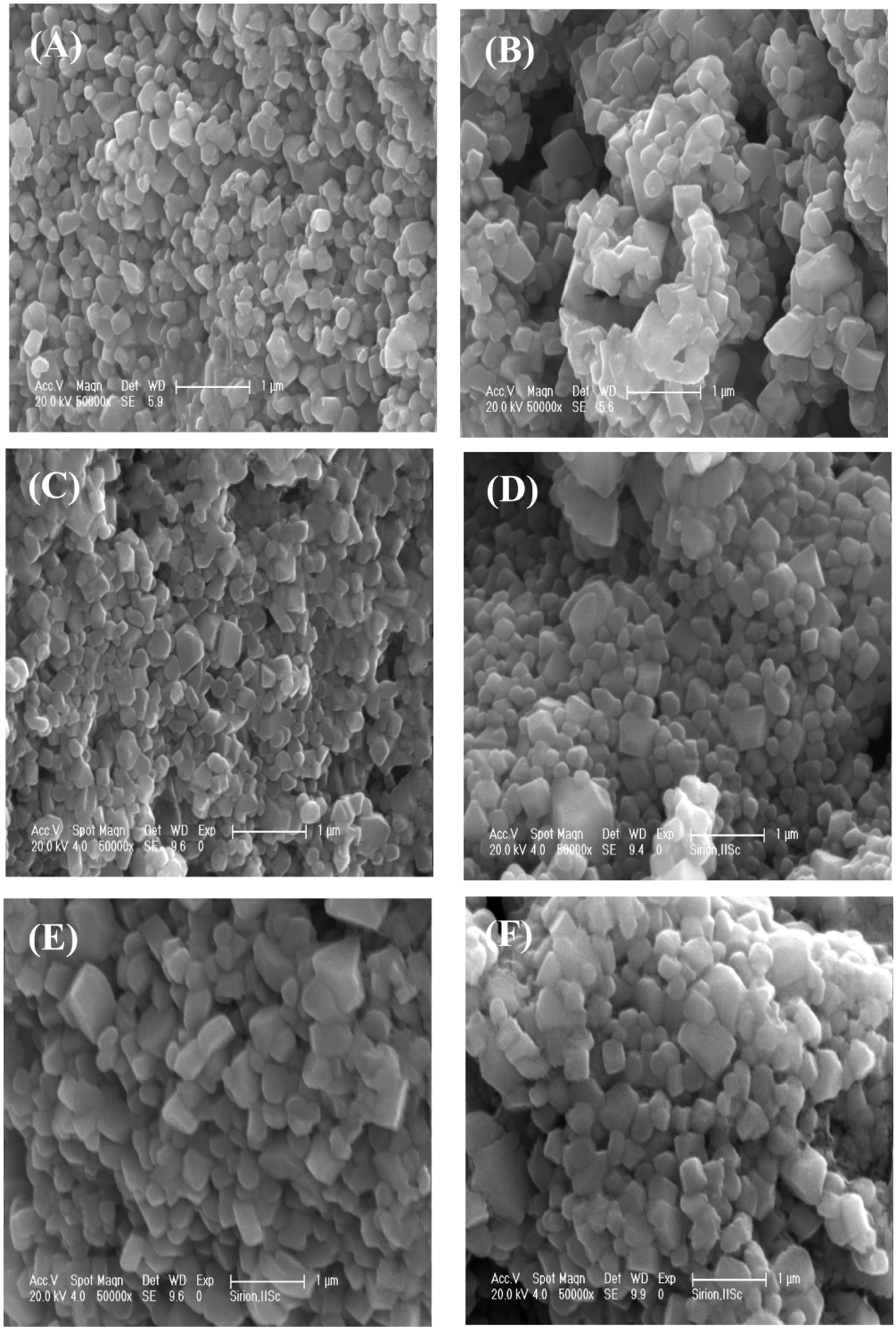


**FIGURE 3. SEM images of $LiNi_{1/3}Co_{1/3}Mn_{1/3}O_2$ (A) C0, (B) C0.1, (C) C0.3, (D) C0.5, (E) C0.75, and (F) C1.0 powder samples.**

formation of a carbon coating on the oxide particles of the C0.75 sample (Figure 4D).

The nitrogen adsorption/desorption isotherms of the C0 and C0.3 samples of $LiNi_{1/3}Co_{1/3}Mn_{1/3}O_2$ are shown in Figure 5. The values of the BET surface area are 2.78 and 5.47 $m^2$ $g^{-1}$ for the C0 and C0.3 samples, respectively. The isotherm of the carbon-coated sample consists of a hysteresis loop at a relative pressure ($P/P_0$) ranging from 0.6 to 0.8, which is a characteristic feature of mesoporous materials. However, the hystersis loop is absent in the adsorption isotherm of the bare sample. Therefore, it can be concluded that a carbon coating increases the surface area of $LiNi_{1/3}Co_{1/3}Mn_{1/3}O_2$, indicative of the porous nature of the carbon-coated layer. Surface area values of the $LiNi_{1/3}Co_{1/3}Mn_{1/3}O_2$ samples prepared by different methods are rarely reported in the literature (27), and these values are very low. For instance, Yoshizawa and Ohzuku (27) reported a value of 0.4 $m^2$ $g^{-1}$ for the samples of $LiNi_{1/3}Co_{1/3}Mn_{1/3}O_2$ prepared by them. In

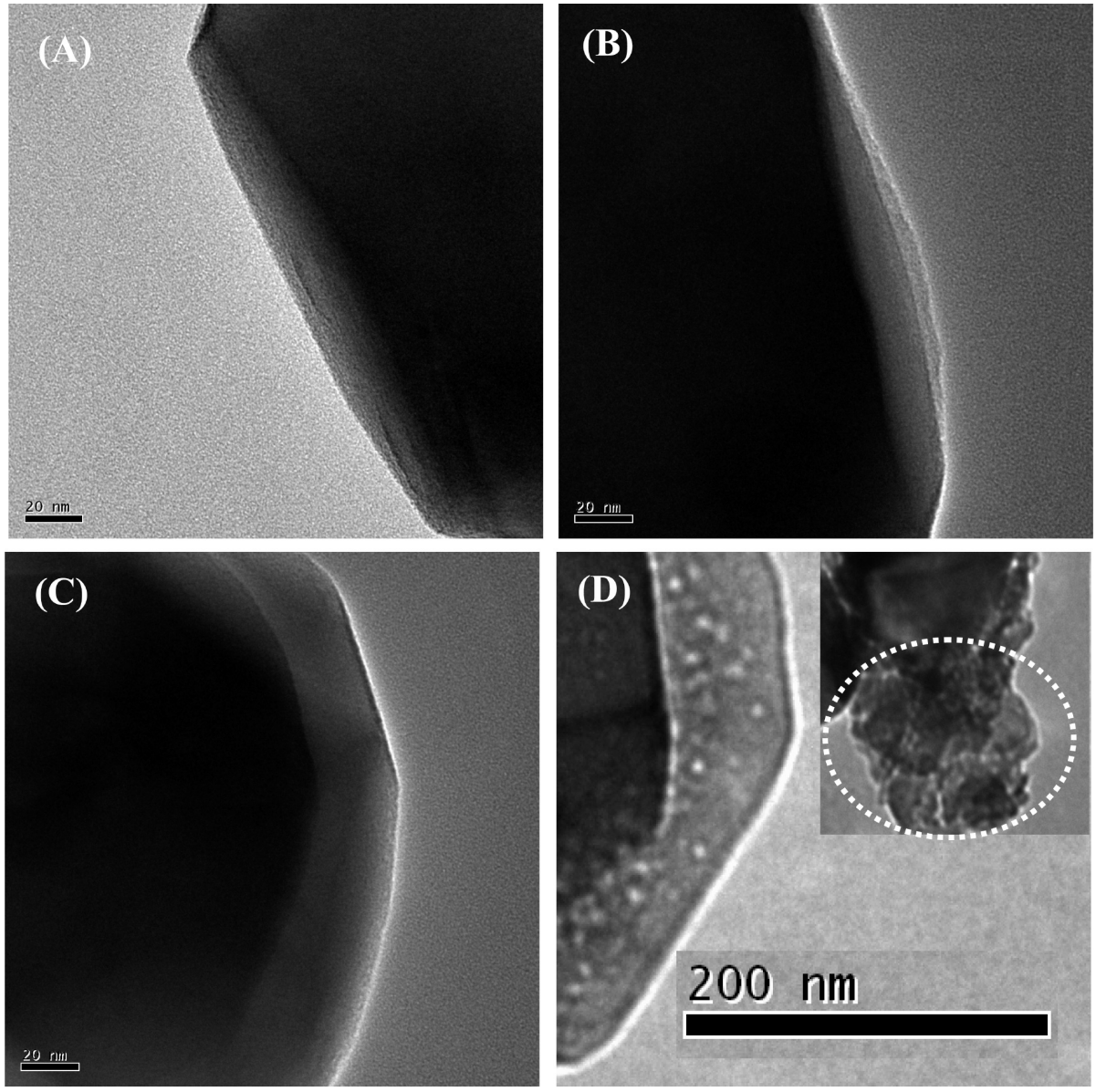


**FIGURE 4. TEM micrographs of the (A) C0, (B) C0.1, (C) C0.3, and (D) C0.75 samples of $LiNi_{1/3}Co_{1/3}Mn_{1/3}O_2$. Free carbon is shown in the inset of part D as the marked area.**

another study, BET surface area values in the range 3.3−3.9 $m^2\ g^{-1}$ are reported for the samples prepared by the spray-drying method (9). In comparison to these studies, the BET area value obtained in the present study, namely, 5.47 $m^2\ g^{-1}$ for the C0.3 sample, is considerably higher. The beneficial effects of carbon coating are also manifested in the generation of a greater surface area for the particles. It is likely that pyrolysis of glucose molecules adsorbed on solid particles during the synthesis causes the formation of a rough surface with carbon coating and therefore a high surface area.

It was reported that the oxidation states of Ni, Co, and Mn are 2+, 3+, and 4+, respectively (4), in $LiNi_{1/3}Co_{1/3}Mn_{1/3}O_2$. The $Ni^{2+}$ and $Co^{3+}$ cations act as the electrochemically active species, which undergo redox transitions, during charge−discharge cycling. $Mn^{4+}$ cations are electrochemically inactive, and they are generally believed to increase the stability of the material framework (4). XPS core spectra of Ni, Co, Mn, and C for the C0 and C0.3 samples are shown in Figure 6. In the Ni $2p_{3/2}$ spectra (Figure 6A) for the C0 and C0.3 samples, the symmetrical peak at a binding energy (BE) of 854 eV corresponds to $Ni^{2+}$ in $LiNi_{1/3}Co_{1/3}Mn_{1/3}O_2$, in agreement with that reported in the literature (28). The Co $2p_{3/2}$ and Mn $2p_{3/2}$ peaks with BE values of 779.5 and 642.2 eV, respectively, correspond to $Co^{3+}$ and $Mn^{4+}$. The presence of $Ni^{2+}$, $Co^{3+}$, and $Mn^{4+}$ in $LiNi_{1/3}Co_{1/3}Mn_{1/3}O_2$ is consistent with that reported in the literature (8), and there is no effect of carbon coating on the oxidation states of transition-metal elements. However, the XPS spectra of C 1s in the C0 and C0.3 samples are different, as shown in Figure 6D. The C 1s spectrum of the C0 sample could be deconvoluted into two peaks, which arise from the carbon tape used for loading of the sample. The peaks present at 285.1 and 287.7 eV are attributed to $sp^2$ C−C and $sp^3$ C−C bonds, respectively (12). However, the C 1s spectrum of the C0.3 sample is deconvoluted into three peaks. The peaks at 285.4 and 286.8 eV

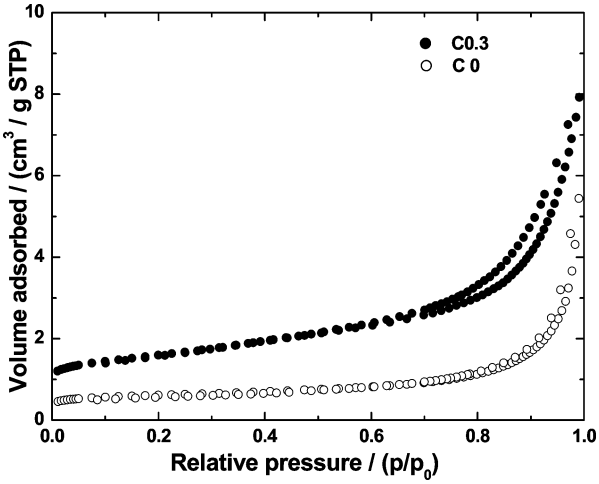


**FIGURE 5. Nitrogen adsorption/desorption isotherms at 77 K of bare C0 and C0.3 samples of $LiNi_{1/3}Co_{1/3}Mn_{1/3}O_2$.**

are due to both the carbon tape and carbon coating on the particles, whereas the third peak at 289.9 eV is attributed to the carbon coating on the $LiNi_{1/3}Co_{1/3}Mn_{1/3}O_2$ particles. This additional peak is due to C−O bond contamination on the surface of the particles (12), which could have taken place during heating of the sample at a high temperature.

Thus, it is clear from the above results that the microemulsion route produced submicrometer-sized particles of $LiNi_{1/3}Co_{1/3}Mn_{1/3}O_2$. Furthermore, the presence of glucose resulted in the formation of carbon as a coating on the particles of the reaction product. Although glucose was present along with the reactants used for the preparation of the compound, its role was limited to generate a coating of carbon on the particles. Formation of the free carbon was noticed at higher levels of glucose. During the synthesis, the oxide ($LiNi_{1/3}Co_{1/3}Mn_{1/3}O_2$) could have crystallized first, followed by decomposition of glucose. While a major part of the glucose could have escaped as $CO_2$ and $H_2O$ due to heating in air at 900 °C, the rest adsorbed on the precursor particles could have formed as a layer of carbon on the particles. Consequently, there was no influence of the glucose on the oxidation states of $Ni^{2+}$, $Co^{3+}$, and $Mn^{4+}$. Furthermore, the layerd structure of $LiNi_{1/3}Co_{1/3}Mn_{1/3}O_2$ was also not disturbed by inclusion of carbon in the crystals. Because of heating in air, the outer layer of the carbon could have been treated with $O_2$, which is evident from the presence of a C−O bond identified from the XPS study.

Figure 7 shows the cyclic voltammogram of a $LiNi_{1/3}Co_{1/3}Mn_{1/3}O_2$ electrode. There is a pair of redox peaks present in the potential range 3.8−3.6 V. This is similar to the features of voltammograms reported in the literature (5). Voltammograms recorded with carbon-coated samples were similar to the voltammogram shown in Figure 7. Among the three transition-metal elements, Ni and Co with oxidation states 2+ and 3+, respectively, are known to be electrochemically active and Mn with oxidation state 4+ is not active. The pair of peaks present in Figure 7 corresponds to the redox transition of $Ni^{2+}/Ni^{4+}$. Current peaks corresponding to $Co^{3+}/Co^{4+}$ are expected to appear at a potential range greater than 4.6 V (4). As the upper limit of the potential in the present study

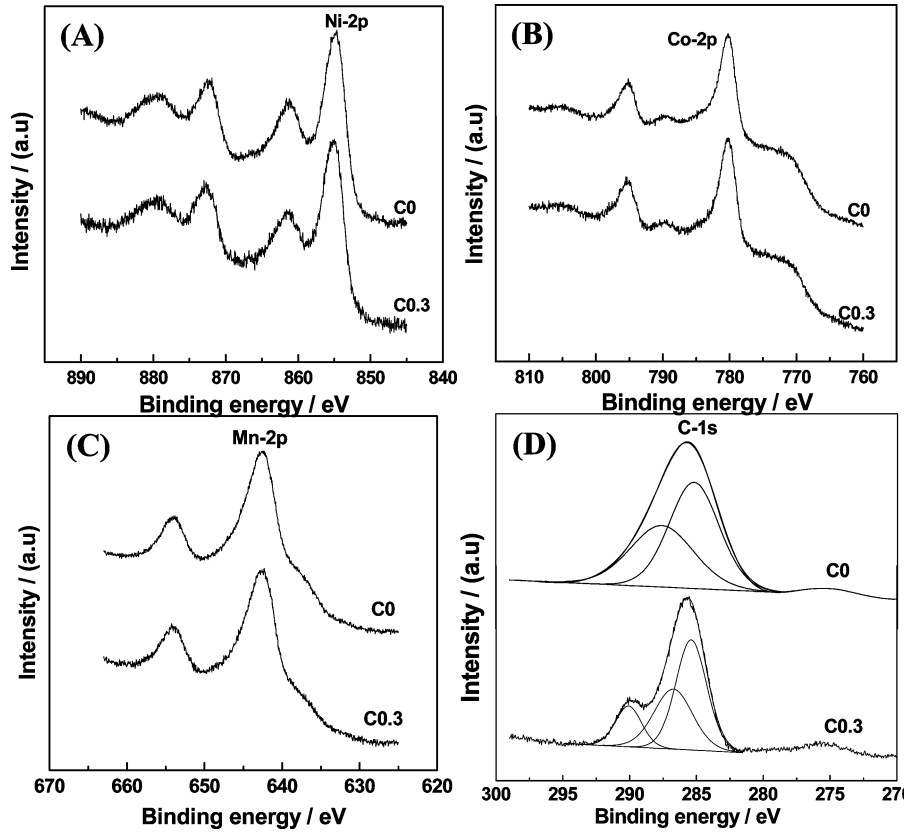


**FIGURE 6. XPS spectra of Ni 2p, Co 2p, Mn 2p, and C 1s for the C0 and C0.3 samples of $LiNi_{1/3}Co_{1/3}Mn_{1/3}O_2$.**

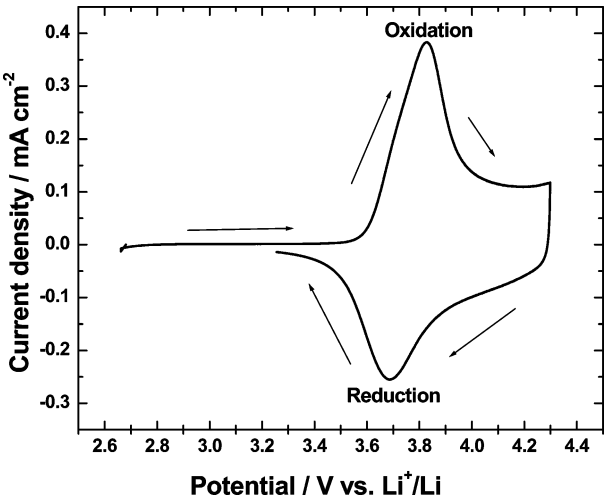


FIGURE 7. Cyclic voltammogram of the carbon-coated C0.3 sample of a $LiNi_{1/3}Co_{1/3}Mn_{1/3}O_2$ electrode at a sweep rate of 0.05 mV $s^{-1}$.

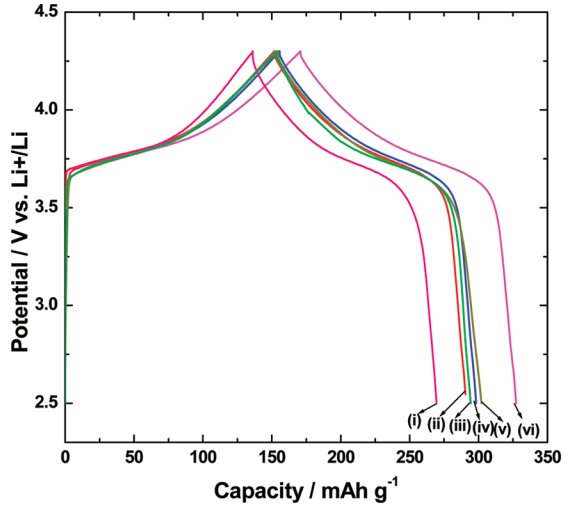


FIGURE 8. Charge–discharge curves of the C0 (i), C1.0 (ii), C0.75 (iii),C0.5 (iv), C0.1 (v), and C0.3 (vi) samples of $LiNi_{1/3}Co_{1/3}Mn_{1/3}O_2$ electrodes at a C/7 rate.

is maintained at 4.3 V, only $Ni^{2+}/Ni^{4+}$ redox peaks are observed in Figure 7.

Charge–discharge curves of $LiNi_{1/3}Co_{1/3}Mn_{1/3}O_2$ electrodes between 2.5 and 4.3 V at a C/7 rate are shown in Figure 8. The midpoint of the plateaus of the charge and discharge curves is around 4.0 V. During discharge, the potential starts decreasing rapidly at about 3.5 V until the end of discharge. The discharge capacity values for C0, C0.1, C0.3, C0.5, C0.75, and C1.0 sample electrodes are 135, 148, 158, 143, 141, and 138 mAh $g^{-1}$, respectively, calculated from the data presented in Figure 8. These values suggest that carbon coating on the $LiNi_{1/3}Co_{1/3}Mn_{1/3}O_2$ particles enhances the discharge capacity, in general, and the C0.3 sample provides the highest capacity, in particular. There is about a 17% increase in the discharge capacity of the C0.3 sample in relation to the capacity of the C0 sample. Thus, the C0.3 sample is considered to possess an optimum level of carbon coating on the oxide particles for achieving a maximum possible discharge capacity. The decrease in the discharge capacity of the C0.5, C0.75 and C1.0 samples in relation to the C0.3 sample is perhaps due to the increased

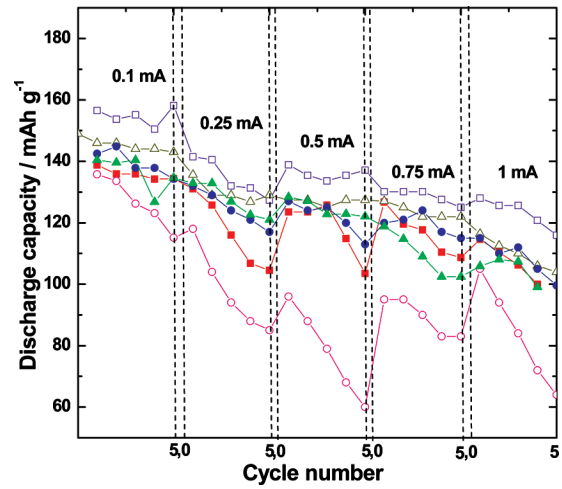


FIGURE 9. Rate capability of the C0 (○), C0.1 (△), C0.3 (□), C0.5 (●), C0.75 (▲), and C1.0 (■) $LiNi_{1/3}Co_{1/3}Mn_{1/3}O_2$ electrodes. For each current used for five consecutive cycles, a fresh electrode was used.

thickness of the carbon coating on the particles of the former sample. A thicker carbon coating can make the particles electronically inactive or can cause coagulation of the particles (29).

To evaluate the rate capabilities of the bare and carbon-coated samples, electrodes were subjected to charge–discharge cycling with different currents and the discharge capacity values are shown in Figure 9. At each current, five charge–discharge cycles were carried out. It is seen that the discharge capacity of the material without carbon coating (C0 sample) is 135 mAh $g^{-1}$ at a current density of 0.1 mA $cm^{-2}$ (23 mA $g^{-1}$), and it decreases to 60 mAh $g^{-1}$ at 1 mA $cm^{-2}$ (153 mA $g^{-1}$). The capacity retention is also very poor during the five cycles at each current. The carbon-coated sample (C0.1) provides 148 mAh $g^{-1}$ at 0.1 mA $cm^{-2}$ current density and 116 mAh $g^{-1}$ at 1 mA $cm^{-2}$. Furthermore, the C0.3 sample electrode provides 156 mAh $g^{-1}$ at 0.1 mA $cm^{-2}$ and 128 mAh $g^{-1}$ at 1 mA $cm^{-2}$. The data of C0.5, C0.75, and C1.0 sample electrodes are also inferior to the data of the C0.3 electrode but superior to the data of the C0 sample. Thus, the C0.3 sample appears to possess an optimum carbon coating. Thus, carbon coating not only improves the electronic conductivity of the active material (30) but also induces a better rate capability.

Figure 10 shows the results of a cycle-life test for the bare and carbon-coated $LiNi_{1/3}Co_{1/3}Mn_{1/3}O_2$ sample electrodes cycled up to 20 cycles at a C/7 rate. The discharge capacity of the carbon-coated C0.3 sample exhibited higher discharge capacity than the rest of the samples. The capacity retention of this sample is better than the rest. Electrochemical data were recorded at different potential ranges and varying rates in the literature (4–10). For instance, Shaju et al. (4) cycled $LiNi_{1/3}Co_{1/3}Mn_{1/3}O_2$ electrodes between 2.5 and 4.4 V at a current density of 30 mA $g^{-1}$. An initial discharge capacity of 160 mAh $g^{-1}$ was obtained during the first cycle, and thereafter it decreased gradually and reached 143 mAh $g^{-1}$ at the end of 40th cycle. A discharge capacity of 157 mAh $g^{-1}$ between 2.7 and 4.2 V at a C/20 rate was reported for microemulsion-derived samples (5). Discharge capacity val-

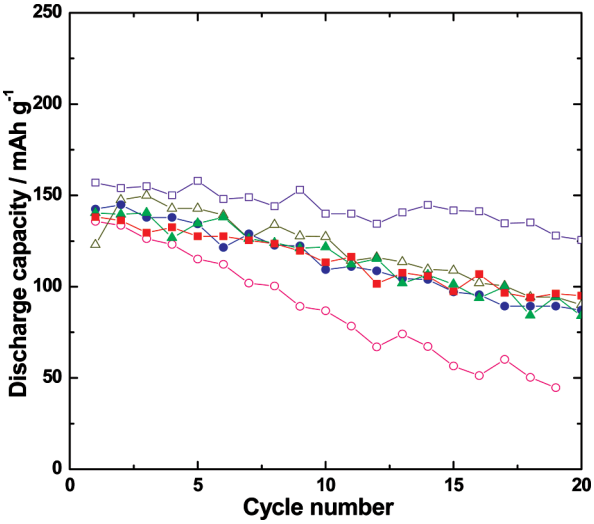


FIGURE 10. Variation of the discharge capacity of C0 (○), C0.1 (△), C0.3 (□), C0.5 (●), C0.75 (▲), and C1.0 (■) $LiNi_{1/3}Co_{1/3}Mn_{1/3}O_2$ electrodes with the cycle number at a C/7 rate.

ues in the range 135−145 mAh $g^{-1}$ between 2.7 and 4.3 V at a current density of 0.055 mA $cm^{-2}$ are reported for $LiNi_{1/3}Co_{1/3}Mn_{1/3}O_2$ samples prepared by two different methods (6). About 155 mAh $g^{-1}$ at a C/5 rate in the potential range 2.5−4.4 V was reported for the sample prepared by a wet chemical process. Capacity values ranging from 151.9 to 188.9 mAh $g^{-1}$ in the potential range 2.5−4.5 V at charge−discharge rates of C/5−4C were reported by Lin et al. (8). The presence of a carbon coating on the particles was shown to improve the capacity retention. Kim et al. (10) reported a discharge capacity of 155 mAh $g^{-1}$ for a carbon-coated sample of $LiNi_{1/3}Co_{1/3}Mn_{1/3}O_2$ in the potential range between 2.8 and 4.3 V. The electrochemical results obtained in the present study reveal that the inverse microemulsion-derived in situ carbon-coated $LiNi_{1/3}Co_{1/3}Mn_{1/3}O_2$ samples provide a high discharge capacity at high rates and good capacity retention.

The Nyquist impedance plots of bare and carbon-coated electrodes are shown in Figure 11. The ac impedance spectra were recorded after five galvanostatic charge−discharge cycles at a C/7 rate in the potential range between 2.5 and 4.3 V. The Nyquist plot consists of a high-frequency intercept and a broad semicircle. The broad semicircle is due to the overlap of two semicircles. The impedance parameters were evaluated by fitting the data to an equivalent circuit using the NLLS fitting program (31). The suitable equivalent circuit, which was found to fit the impedance data, is shown as the inset of Figure 11. The two semicircles are due to two pairs of parallel resistance and capacitance (32). Because the semicircles are depressed with their centers below the real axis, capacitors are replaced by a constant phase element (CPE, $Q$) (33). Similar to the data of the $LiNi_{1/3}Co_{1/3}Mn_{1/3}O_2$ electrode obtained in the present study, impedance of $LiCoO_2$ was shown to consist of two semicircles (34). It was concluded that the formation of a surface layer on $LiCoO_2$ was responsible for the high-frequency semicircle and the kinetics of intercalation/deintercalation of lithium in the electrode for the low-frequency semicircle. Accordingly, $R_1$ is the resistance

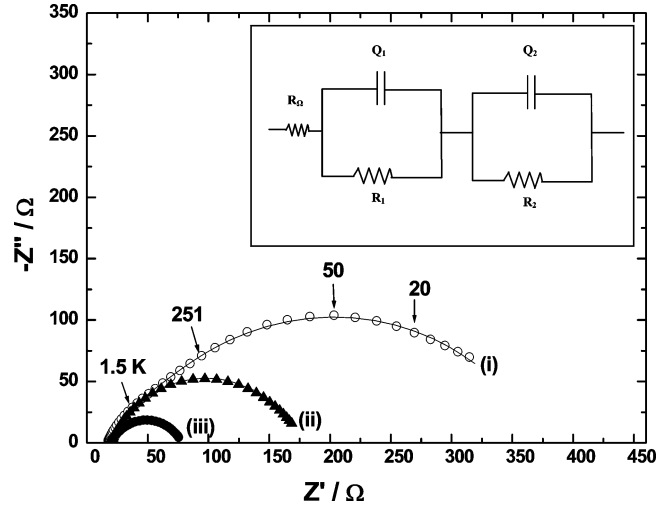


FIGURE 11. Nyquist plots of C0 (i), C0.1 (ii), and C0.3 (iii) samples of $LiNi_{1/3}Co_{1/3}Mn_{1/3}O_2$ electrodes at room temperature. Experimental data are shown as open circles, and theoretical data obtained from fitting are shown as curves. The frequencies of some data points are given in hertz. Inset: Equivalent circuit used for NLLS fitting of the experimental impedance data [$R_\Omega$ = ohmic resistance; $R_1$ = surface-film resistance; $Q_1$ = CPE of the surface film; $R_2$ = charge-transfer resistance ($R_{ct}$), and $Q_2$ = CPE of the double layer].

of the surface film on an oxide electrode and $Q_1$ is a CPE corresponding to the surface film capacitance. The impedance parameters, $R_2$ and $Q_2$, are resistance and CPE, respectively, corresponding to the electrochemical intercalation/deintercalation process and double-layer capacitance. The impedance parameters were obtained by fitting the data (Figure 11) to the equivalent circuit. The resistance $R_2$ corresponds to intercalation/deintercalation of $Li^+$ into/from the electrodes, and it is equivalent to the charge-transfer resistance ($R_{ct} = R_2$) of the electrochemical process. The charge-transfer resistance of the carbon-coated C0.3 sample is the least at 43.1 Ω compared to the other samples, i.e., 129.7 Ω for the C0.1 sample and 340.5 Ω for the C0 sample electrodes. Thus, the beneficial effect of a carbon coating on the particles of $LiNi_{1/3}Co_{1/3}Mn_{1/3}O_2$ is reflected in the impedance measurements.

## CONCLUSIONS

Carbon-coated submicrometer-sized particles of $LiNi_{1/3}Co_{1/3}Mn_{1/3}O_2$ in a single pot using an inverse microemulsion medium in the presence of glucose. The precursor obtained from the reaction is heated at 900 °C for 6 h to get crystalline $LiNi_{1/3}Co_{1/3}Mn_{1/3}O_2$. The carbon coating is found to impart to porosity as well as a higher surface area in relation to bare samples of the compound. The electrochemical characterization studies provide that carbon-coated $LiNi_{1/3}Co_{1/3}Mn_{1/3}O_2$ samples exhibit improved rate capability and cycling performance. The carbon coatings are shown to suppress the capacity fade, which is normally observed for the bare compound. Impedance spectroscopy data provide additional evidence for the beneficial effect of a carbon coating on $LiNi_{1/3}Co_{1/3}Mn_{1/3}O_2$ particles.

**Acknowledgment.** The authors thank Ms. Nimisha and Prof. G. Mohan Rao for XPS studies.

## REFERENCES AND NOTES


(1) Nazri, A.; Pistoia, G. *Lithium Batteries: Science and Technology*; Kluwer: Boston, 2004; p 1.
(2) Mizushima, K.; Jones, P. C.; Wiseman, P. J.; Goodenough, J. B. *Mater. Res. Bull.* **1980**, *15*, 783.
(3) Ohzuku, T.; Makimura, Y. *Chem. Lett.* **2001**, *7*, 642.
(4) Shaju, K. M.; Rao, S.; Chowdari, B. V. R. *Electrochim. Acta* **2002**, *48*, 145.
(5) Ge, T. D.; Yu, L. Q.; Ni, W. N.; Dong, T. A.; Xing, T. L.; Long, H. K.; Yang, J. X. *Mater. Chem. Phys.* **2005**, *94*, 423.
(6) Patoux, S.; Doeff, M. M. *Electrochem. Commun.* **2004**, *6*, 767.
(7) Li, D. C.; Muta, T.; Zhang, L. Q.; Yoshio, M.; Noguchi, H. *J. Power Sources* **2004**, *132*, 150.
(8) Lin, B.; Wen, Z. J.; Han, W. X. *Solid State Ionics* **2008**, *179*, 1750.
(9) Li, X.; Wei, Y. J.; Ehrenberg, H.; Du, F.; Wang, C. Z.; Chen, G. *Solid State Ionics* **2008**, *178*, 1969.
(10) Kim, H. S.; Kim, K.; Moon, S. I.; Kim, I. J.; Gu, H. B. *J. Solid State Electrochem.* **2008**, *12*, 867.
(11) Kim, H. S.; Kim, Y.; Kim, S. I.; Martin, S. W. *J. Power Sources* **2006**, *161*, 623.
(12) Guo, R.; Shi, P.; Cheng, X.; Du, C. *J. Alloys Compd.* **2008**, in press.
(13) Kim, H.-S.; Kong, M.; Kim, K.; Kim, I.-J.; Gu, H.-B. *J. Power Sources* **2007**, *171*, 917.
(14) Li, J.; He, X.; Zhao, R.; Wan, C.; Jiang, C.; Xia, D.; Zhang, S. *J. Power Sources* **2006**, *158*, 524.
(15) Kim, G. H.; Kim, M. H.; Myung, S. T.; Sun, Y. K. *J. Power Sources* **2005**, *146*, 602.
(16) Kim, G. H.; Myung, S. T.; Kim, H. S.; Sun, Y. K. *Electrochim. Acta* **2006**, *51*, 2447.
(17) Kim, Y.; Kim, H. S.; Martin, S. W. *Electrochim. Acta* **2006**, *52*, 1316.
(18) Huang, H.; Yin, S. C.; Nazar, L. F. *Electrochem. Solid State Lett.* **2001**, *4*, A170.
(19) Cushing, B. L.; Goodenough, J. B. *Solid State Sci.* **2002**, *4*, 1487.
(20) Marcinek, M. L.; Wilcox, J. W.; Doeff, M. M.; Kostecki, R. M. *J. Electrochem. Soc.* **2009**, *156*, A48.
(21) Cushing, B. L.; Kolesnichenko, V. L.; O'Connor, C. J. *Chem. Rev.* **2004**, *104*, 3893.
(22) Sinha, N. N.; Munichandraiah, N. *J. Solid State Electrochem.* **2008**, *12*, 1619.
(23) Kim, J.; Park, C.; Sun, Y. *Soild State Ionics* **2003**, *164*, 43.
(24) Ohzuku, T.; Ueda, A.; Nagayama, M.; Iwakoshi, Y.; Komori, H. *Electrochim. Acta* **1993**, *38*, 1159.
(25) Reimers, J. N.; Rossen, E.; Jones, C. D.; Dahn, J. R. *Solid State Ionics* **1993**, *61*, 335.
(26) Han, A. R.; Kim, T. W.; Park, D. H.; Hwang, J.-S.; Choy, J.-H. *J. Phys. Chem. C* **2007**, *30*, 11347.
(27) Yoshizawa, H.; Ohzuku, T. *J. Power Sources* **2007**, *174*, 813.
(28) Briggs, D., Seah, M. P., eds. *Practical Surface Analysis by Auger and X-ray Photoelectron Spectroscopy*; John Wiley & Sons: Chichester, U.K., 1983; p 519.
(29) Chen, Y.; Dahn, J. R. *J. Electrochem. Soc.* **2002**, *149*, A1148.
(30) Wang, G. X.; Yang, L.; Bewlay, S. L.; Chen, Y.; Liu, H. K.; Ahn, J. H. *J. Power Sources* **2005**, *146*, 521.
(31) Boukamp, B. A. *Equivalent Circuit: Users Manual*; University of Twente: Enschede, The Netherlands, 1989; p 1.
(32) Rodrigues, S.; Munichandraiah, N.; Shukla, A. K. *J. Power Sources* **2002**, *87*, 12.
(33) Macdonald, J. R. *Impedance Spectroscopy*; Wiley: New York, 1987; p1.
(34) Thomas, M. G. S. R.; Bruce, P. G.; Goodenough, J. B. *J. Electrochem. Soc.* **1985**, *132*, 1521.


AM900120S